Assessing the Reactive Surface Area of Phlogopite during Acid Dissolution: An Atomic Force Microscopy, X-ray Photoelectron Spectroscopy, and Low Energy Electron Diffraction Study

Eric S. Rufe

Thesis submitted to the Faculty of Virginia Polytechnic Institute and State University in partial fulfillment of the requirements for the degree of

Master of Science
In
Geological Sciences

Michael F. Hochella, Jr., Chair
Robert J. Bodnar
J. Donald Rimstidt

January 14, 2000
Blacksburg, Virginia

Keywords: AFM, XPS, LEED, phlogopite, reactive surface area

Assessing the Reactive Surface Area of Phlogopite during Acid Dissolution: An Atomic Force Microscopy, X-ray Photoelectron Spectroscopy, and Low Energy Electron Diffraction Study

Eric S. Rufe

Abstract

The behavior during dissolution of edge and basal surfaces of the mica phlogopite were examined using in situ atomic force microscopy (AFM), x-ray photoelectron spectroscopy (XPS) and low-energy electron diffraction (LEED) in an attempt to characterize the reactive surface area during dissolution. Mica minerals are the ideal material for this study because they offer a high degree of structural anisotropy. Therefore surfaces with different structures are easily identified. Dissolution is shown to proceed preferentially by removal of material from {hk0} edges. Dissolution rates were calculated by measuring the volume of material removed from etch pits, and normalizing to either the "reactive" surface area of {hk0} edges exposed at pit walls, or to a total "BET-equivalent" surface area. Rates normalized to total surface area are in the range of dissolution rates reported in the literature. Edge surface normalized rates are about 100 times faster. Long-term in situ AFM observations of phlogopite dissolution reveal that exposed (001) surfaces also display a distinct reactivity, though it operates on a different time scale. The top layer is shown to expand between 39 and 63 hours in contact with pH 2 HCl solution. Subsequent LEED analysis shows that the (001) surface becomes amorphous upon reacting with pH 2 HCl. Compositional characterization of the phlogopite after reaction shows that for pitted phlogopite surfaces, dissolution is characterized by leaching of octahedral cations and polymerization of the silica-enriched residual layer. No chemical changes or polymerization are observed for freshly cleaved unpitted phlogopite after reaction with pH 2 HCl for 24 hours. This suggests a gallery access mechanism is facilitated by edge attack, and is only significant on exposed (001) surfaces after a certain amount of dissolution by edge attack.

Acknowledgements

First I would like to thank my advisor Mike Hochella for all of the support, guidance, friendship and patience (especially patience) he has given me during the time I have spent here at Tech.

Several professors have been extremely helpful discussing ideas and making their time and facilities available to me. I especially thank Don Rimstidt and Bob Bodnar in this regard.

My colleagues in the Fifth Floor geochemistry group have been a constant source of inspiration, support and friendship. They have helped to make this time fun and productive. I thank especially Barry Bickmore, Udo Becker, Kevin and Jodi Rosso, Dirk Bosbach, Erich Weissbart, Russ Able, Rob Weaver, Steven Lower, Djinni Jerz, Erin O'Reily and Treavor Kendall.

Many people have provided technical assistance, good ideas and help running machines. I thank especially Todd Solberg, Dan Smith, Mark Fortney, Frank Cromer, Frank Harrison and Jing Leng.

I am grateful to Linda Bland, Connie Lowe, Mary McMurray and Carolyn Williams for the friendship and help they have given through the years. Without them, I quite literally would not have made it through.

Also, I am grateful to all the friends I have made in the department through the years-too many to name-especially Brian Coffey and Peter Welch, who understand the value of arcade video games.

Most of all, I thank my wife, Maria, who has been a constant source of love, support and balance.

Table of Contents

List of Figures

List of Tables

Chapter 1: INTRODUCTION

1.1 Overview of Reactive Surface Area

Silicate dissolution has been a topic of intense geochemical research over the past several decades. Yet kinetic studies of dissolution rates can vary significantly from laboratory to laboratory, and between the laboratory and the field. One of the greatest unknowns in these studies is how to most appropriately quantify and express the surface area measurements that rates are normalized to. It has been suggested that some positions of a mineral surface are inherently "more reactive" than others, by virtue of crystallographic structure, microtopography, defect density or hydrologic coupling. This research was designed to serve as a starting point to begin assessing the different types of surface reactivates. Specifically, the reactivity of phlogopite {001} surfaces was compared directly to {hk0} surfaces. Mica minerals are the ideal starting point for this line of research because they have a high degree of structural anisotropy that allows for simple determination of different surfaces with greatly differing reactivity.

Phlogopite dissolution rates are measured by analysis of AFM images captured in situ. This represents one of the first direct measurements of silicate dissolution occurring in real time. By measuring the edge surface area of etch pits nucleated on the (001) surface, dissolution rates are normalized to "reactive surface area". Additionally, by constructing imaginary particles with the same dimensions as the etch pits, it is possible to measure a "BET-equivalent" surface area. This allows dissolution rates measured in situ by AFM to be compared directly to rates reported from solution studies with some degree of success. Long-term, in situ AFM observations also indicate the (001) surfaces have a distinct reactivity.

1.2 Looking Ahead

This research is a first attempt at understanding the nature of "reactive" surface area. Studies like this are necessary to determine the reactivity of different crystallographic faces. However, mica minerals represent the ideal case for this type of examination. Greater challenges lie ahead for the investigation of silicates with poor cleavages, such as feldspars. Additionally, future studies will need to characterize not only the proportion and relative reactivity of various

crystallographic faces, but will also need to characterize the proximal flow regimes, and the density and distribution of topographic features and defects.

1.3 Introduction

Chemical weathering of silicate minerals exerts substantial influences on processes such as neutralization of anthropogenic acidic inputs, supplying and cycling of nutrients in natural systems, and long-term climate change by acting as a sink for atmospheric CO_2 (White and Brantley, 1995, and references therein). Laboratory and field-based studies that determine dissolution rates rely on measurements of exposed mineral surface area, but unfortunately, surface area remains one of the most difficult parameters to characterize. Most often, laboratory rates are normalized to initial surface area measured by a Brunaer-Emmett-Teller (BET) adsorption isotherm. For many silicates, no linear relationship exists between rate and BET surface area, implying that not all of the measured surface area participates in the reaction at the same rate or by the same mechanism (Brantley and Chen, 1995; White and Peterson, 1990). The term "reactive surface area" is often used to distinguish the portions of the surface that dominantly contribute to measured fluxes from portions that do not. In the literature, the way in which reactive surface area is defined is variable. Some authors define reactive surface area as the area occupied by high-energy sites, such as defects and dislocation outcrops (Casey et al., 1988). In surface complexation modeling, reactive sites consist of particular atomic arrangements where ligand adsorption and activated complex formation occurs (Koretsky et al., 1998). Microscopic studies of the mineral-solution interface indicate that coordinatively unsaturated microtopographic configurations, such as kinks and steps, comprise the most reactive portion of a mineral surface (Hochella, 1995). In field based studies, reactive surface area is the portion of the total mineral surface area that is in hydrologic contact with the system under study (Drever and Clow, 1995).

To gain insight into the intricacies of mineral dissolution, others have used in situ atomic force microscopy (AFM) to examine reactions in real time on particular crystallographic faces or microtopographic features of several non-silicate minerals (Jordan and Ramansee, 1996; Liang et al., 1995; Putnis et al., 1995). However, real time AFM imaging of silicate minerals has been

limited, owing to the slow dissolution rates of these minerals. Therefore, previous AFM investigations of silicate dissolution have been limited to ex situ experiements (Hochella et al, 1998). This study combines in situ AFM observations of the dissolution of the mica phlogopite [$K_2Mg_6(Al_2Si_6O_{20})(OH,F)_4$] at room temperature with x-ray photoelectron spectroscopy (XPS) and low-energy electron diffraction (LEED) analyses to quantitatively assess reactive surface area. Phyllosilicates are particularly well-suited to this type of study because they possess a high degree of structural anisotropy. As a result, different crystallographic faces might be predicted to have widely varying reactivates. For example, Turpault and Trotignon (1994) examined the differential reactivity of macroscopic biotite flakes with varying proportion of edge to basal surface area and found that the {hk0} edges are apparently about 250 times more reactive than {001} in pH 1 HNO_3 solution. It has generally been concluded that mica dissolution is dominated by an edge attack mechanism, whereby octahedral and interlayer cations are removed through the {hk0} edges, parallel to the {001} layers (Malmstrom and Banwart, 1997; Kalinowski and Schweda, 1996; Nagy, 1995 and references therein). Evidence for this mechanism is provided by initial preferential release of octahedral and interlayer cations, and by the dependence of hydrolysis rates on particle size of clays (Cetisli and Gedikbev, 1990). More recently, direct observations of phyllosilicate dissolution in the fluid cell of atomic force microscopes (AFMs) point to the same conclusion, that is that phyllosilicate dissolution proceeds preferentially by removal of material from {hk0} surfaces (Bickmore et al, 2000; Rufe and Hochella, 1999; Bosbach et al, 1999). Furthermore, the reactivity of different {hk0} faces of clay minerals has been determined by in situ AFM analysis (Bickmore et al, 2000; Bosbach et al, 1999).

Generally, mica (001) surfaces are regarded as inert during dissolution process (Nagy, 1995). However, a gallery access mechanism has been proposed whereby octahedral cations are leached through the ditrigonal cavities of the tetrahedral sheet, perpendicular to the (001) surface. This mechanism has been demonstrated during late stages of dissolution of expandable flurohectorite clay (Kaviratna and Pinnavaia, 1994). After significant depletion of octahedral Mg (i.e removal of about 2/3 of initial octahedral Mg), the authors noted loss of X-ray diffraction patterns of fluorohectorite in 0.5 M HCl at 60º. Kaviratna and Pinnavia (1994) suggest that gallery access becomes significant only in the late stages of hydrolysis because edge attack

becomes inhibited by the formation of silica-enriched reaction products at the particle edges, slowing the rate of diffusion of octahedral cations. Alternately, the authors propose that gallery access is facilitated by the structural disorder induced by edge attack.

Chapter 2: MATERIALS AND METHODS

2.1 Samples

For this study, two phlogopite samples were examined. A natural phlogopite from Burgess, Ontario (Sample # HB-1246, obtained from the Museum of Geological Sciences at Virginia Tech), and synthetic fluorophlogopite (McCauley, 1973; Bloss, et al., 1963). Major element analysis was performed using a Cameca SX-50 electron microprobe. Standardization was performed on silicate and simple oxide standards, and data reduction was performed according to the "PAP" procedure of Pouchou and Pichoir (1985). All samples were analyzed at 15 kV and 20 nA with 10 mm beam diameter. A total of ten analyses were collected at several locations, and no significant compositional zoning was detected. Formulas were calculated based on (O+OH+F)=24. The synthetic fluorophlogopite is essentially ideal end-member composition: $(K_{0.81}(Mg_{2.86}Al_{0.13}Fe_{0.01})Al_{0.89}Si_{3.11})O_{10}(OH_{0.39}F_{1.61})$. The natural phlogopite contains some excess Al substituting for Mg and a significant amount of F in the octahedral sheet and has the following formula: $(K_{0.84}Na_{0.03}(Mg_{2.58}Al_{0.213}Fe_{0.11}Mn_{0.02})Al_{0.984}Si_{3.06}Ti_{0.07})$-$O_{10}(OH_{1.30}F_{0.69}Cl_{0.01})$. Samples were freshly cleaved into thin sheets (<0.1 mm thick) after being cut into approximately 1 cm^2 pieces. Samples that received HF pre-etching (to generate etch pits; see below) were immersed in 49% HF for 3 s, thoroughly rinsed in a stream of distilled-deionized water, and blown dry with a stream of compressed N_2.

2.2 Atomic Force Microscopy

AFM images were collected with an Extended Multimode atomic force microscope with a Nanoscope IIIa controller (Digital Instruments, Santa Barbara, CA). After initial etching, phlogopite samples were placed in the AFM fluid cell. Solutions of pH 2 HCl or pH ~5.7 distilled, deionized water equilibrated with atmospheric CO_2 were introduced with a syringe and pumped at 10 ml/hr with a low flow peristaltic pump. Pumping was suspended during image acquisition. AFM images were collected in fluid operating in Tapping Mode, using oxide sharpened SiN probes. After engaging, several images were collected in succession and compared to check for scanner drift, tip induced sample erosion, and changes in tip geometry. When not collecting images, the AFM probe was withdrawn to reduce the potential for tip

induced erosion of the sample surface. Standard thresholding image analysis routines were performed on the AFM images to measure the cross-sectional area, perimeter and volume of each etch pit imaged (Barrett et al., 2000; Bickmore, et al., 1999; Russ, 1999).

2.3 X-ray Photoelectron Spectroscopy

XPS measurements were performed using a Perkin-Elmer 5400 (PHI) x-ray photoelectron spectroscopy system equipped with a concentric hemispherical analyzer and dual anode (Al, Mg) X-ray source operating at a base pressure of $5x10^{-7}$ mbar. Photoelectrons were generated using non-monochromatic Al K_α radiation ($h\nu$=1486.0 eV). Survey spectra were collected from 0 to 1000 eV with a pass energy of 44.75 eV and a step size of 1.0 eV. Narrow scans were collected with a pass energy of 17.9 eV and step size of 0.1 eV. The following photolines were analyzed: K 2p, Si 2p, Al 2p, Mg 2s, O 1s, F 1s and C 1s. Although carbon is not a component of the minerals under study, adventitious carbon contamination is ubiquitous in XPS analyses, and the C 1s spectra were collected to assess the degree of contamination on the samples. Qualitative depth profiling was achieved by tilting the sample relative to the photoelectron detector (Hochella, 1988). Photoelectrons were collected at 15°, 45° and 90° take-off angle. Assuming an approximate attenuation length for photoelectrons in a silicate matrix and within the kinetic energy range of interest is about 2.5 nm (see Hochella and Carim, 1988), these angles correspond to analytical depths of approximately 2.0, 5.0 and 7.5 nm.

Semi-quantitative atomic ratios were determined from measured peak intensities (Hochella, 1988). Sensitivity factors were determined by measuring relative peak intensities of the compositionally well-constrained synthetic fluorophlogopite sample. Peak intensities were measured using the SPDv2 software (XI International), after applying a Shirley-type background. Peak fitting was performed using Gaussian peak shapes. Sensitivity factors for all photolines except Mg 2s agree well with the sensitivity factors reported by Wagner et al. (1982. The Mg 2s sensitivity factor determined in this study is about 30% lower than that reported by Wagner et al. (1982). Absolute binding energies of photopeaks were referenced using the K $2p_{3/2}$ photoline as an internal standard. The absolute binding energy K $2p_{3/2}$ photoline was found

to be 293.12 eV relative to the Au $4f_{7/2}$ photoline at 84.0 for gold sputtered on a sample of natural phlogopite following the procedures and precautions of Stipp and Hochella (1992).

2.4 Low Energy Electron Diffraction

Low energy electron diffraction (LEED) spot patterns were collected with four-grid reverse view LEED optics (OMICRON, Taunusstein, Germany) at beam energies between 50 eVand 150 eV. The electron gun has a beam diameter of approximately 1 mm. LEED spot patterns were recorded photographically.

Chapter 3: RESULTS AND DISCUSSION

3.1 Morphology of etched phlogopite (001) surfaces

AFM images provide topographic information about the abundance of different surfaces on HF etched phlogopite (001). Freshly cleaved mica (001) surfaces are typically atomically smooth, with occasional cleavage steps that are multiples of the 1.0 nm 2:1 layer height. HF etching produces triangular, crystallographically controlled etch pits (c.f. Patel and Ramanathan, 1962a; Medina, et al., 1985). Two distinct etch pit populations form during this treatment (Figure 1). Most etch pits are 1.0 nm deep. Deeper etch pits (up to 20 nm deep) are less common. These different types of etch pits are thought to nucleate on different types of defects (Patel and Ramanathan, 1962b). The shallow (1.0 nm) etch pits nucleate on compositional point defects. Hence, once the defect has been removed, dissolution in the [001] direction ceases. Deeper etch pits nucleate on linear defects, allowing for deeper penetration perpendicular to the (001). It is impossible to control the initial density of etch pits during HF etching because the pit density depends on the defect density. The remaining top (001) surface remains atomically smooth. Since 1.0 nm deep pits are more prevalent than deeper pits, the top T-O-T layer has large edge surface area exposed in the etch pit walls. Deeper T-O-T layers have less edge surface area exposed. Note that the top layer has surface area exposed to solution along the topmost (001) surface and (hk0) edges of shallow etch pits. Deeper layers have only (hk0) edges exposed along the walls of deep etch pits, and (001) surfaces exposed at the floors of etch pits.

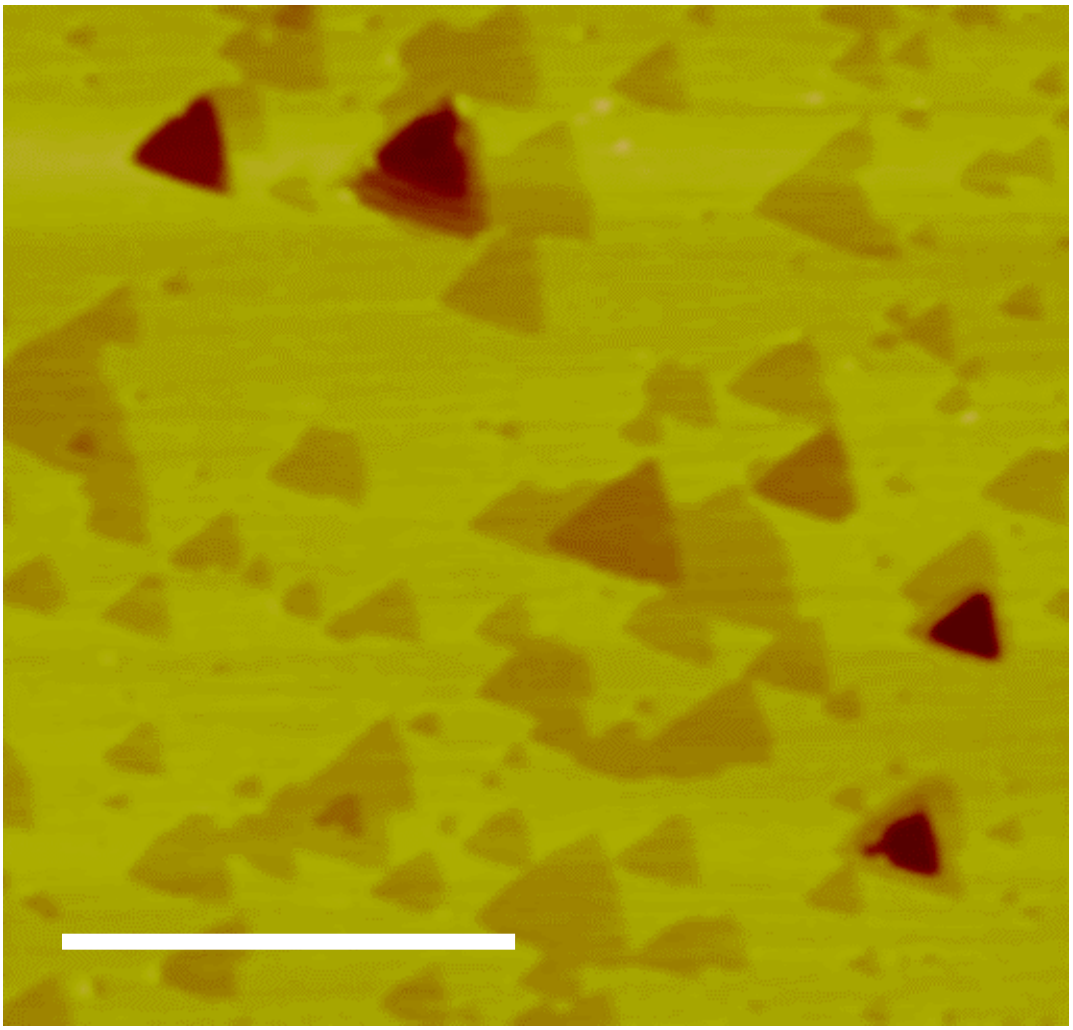

Figure 1: AFM image of typical morphology observed on HF etched phlogopite (001). Scale bar is 1 □m. Each step in this image is 1.0 nm deep, corresponding to one fundamental T-O-T layer in the phlogopite structure.

3.2 LEED Observations

Low energy electron diffraction provides information about the degree of crystallinity of the near surface region of a well-ordered sample. For silicate minerals, the sampling depth is approximately 0.5-0.7 nm. Freshly cleaved phlogopite produces a pattern of diffraction spots consistent with the bulk (001) structure of phlogopite (Figure 2A). Phlogopite samples that received HF pre-etching also showed diffraction spots consistent with the freshly cleaved phlogopite (Figure 2B). However, the diffraction spots appeared with lower intensity. Similarly, freshly cleaved phlogopite that was exposed to identical rinsing (but not HF etching) also showed diffraction patterns with lower intensity (Figure 2C). We attribute the decreased intensity of these patterns to an amorphous overlayer of carbon-containing adventitious material originating in the air and/or water that contacted the samples during preparation. LEED performed on a sample of HF etched phlogopite after 127 hours in contact with pH 2 HCl solution yielded no diffraction spots, indicating that at least the top 5-7 Å of the sample became amorphous.

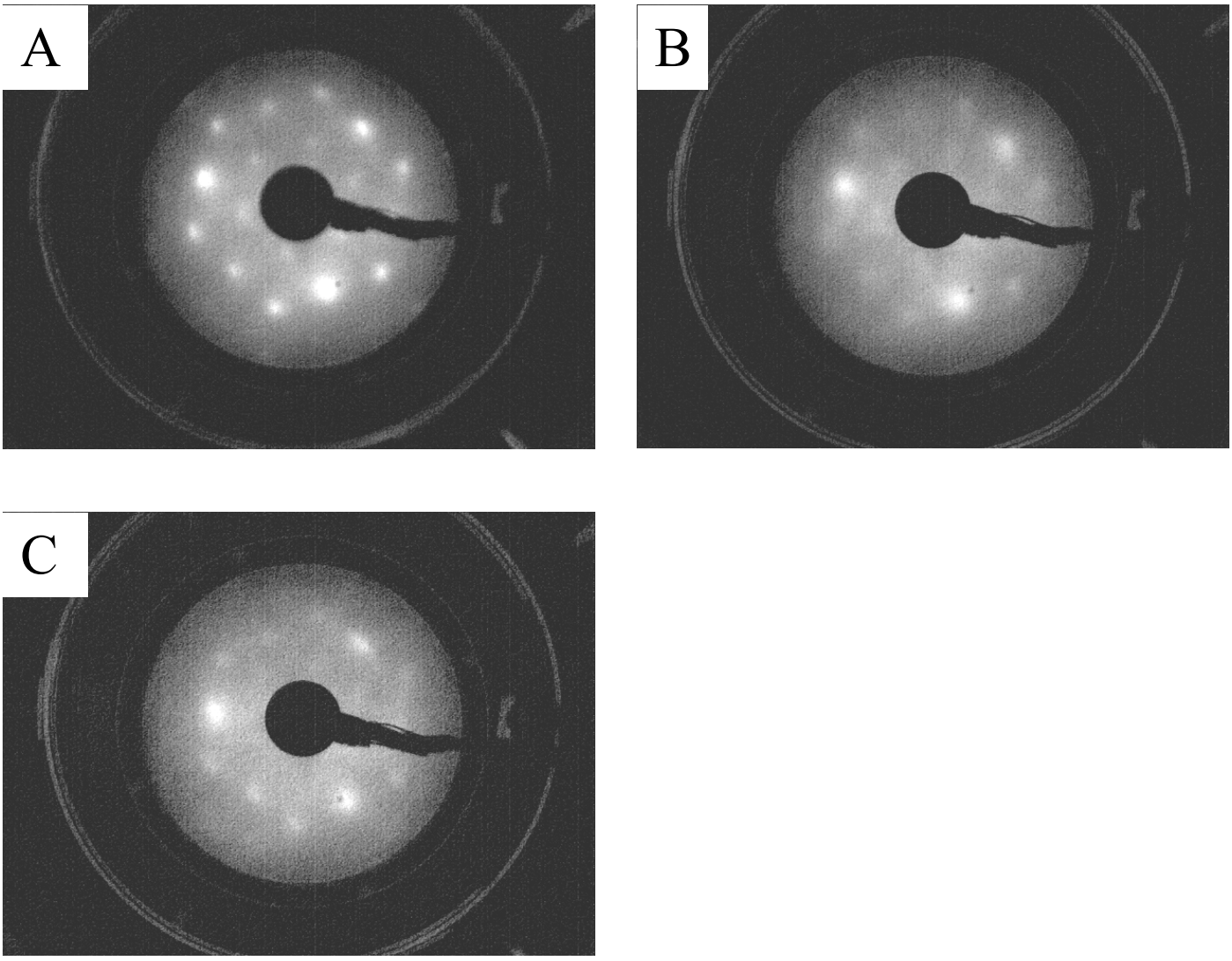

Figure 2: LEED Spot Patterns of phlogopite (001) surfaces receiving the following treatment: (A) cleaved immediately before placing in vacuum, (B) freshly cleaved followed by HF etching and rinsing, (C) freshly cleaved followed by rinsing (no HF etching).

C

3.3 Acid Dissolution of etched phlogopite (001) surfaces

AFM images of the etched phlogopite (001) surface show that dissolution proceeds by removal of material from the etch pit walls (Fig. 3). Etch pits retain the same morphology while dissolving, indicating that each etch pit wall retreats at essentially the same rate. Additionally, no new etch pits nucleate on {001} surfaces. The region of the surface was imaged at various times over the course of several days, and the cross-sectional area, perimeter and volume of each etch pit was measured at each time interval. These values are reported in Table 1 for measurements made in pH 2 HCl, and Table 2 for measurements made in pH 5.7 distilled, deionized water equilibrated with atmospheric CO_2. XPS analysis shows decreasing K/Si, Al/Si, Mg/Si and F/Si atomic ratios within the first 24 hours of reaction, consistent with the observations of incongruent dissolution occurring during dissolution of phyllosilicates in acidic solution. Since Mg, Al and K are preferentially removed with respect to Si, the dissolution rates determined from these AFM observations are compared to dissolution rates calculated from Si release reported in solution studies. Dissolution rates were calculated as follows:

$$Rate = \frac{(\Delta V / V_m)}{A \cdot \Delta t} \quad \textbf{[mole m}^{-2}\textbf{ sec}^{-1}\textbf{]} \qquad \textbf{(1)}$$

where ΔV is the volume of phlogopite removed from the etch pit, V_m is the molar volume of the phlogopite (based on a complete formula unit), Δt is the time interval and A is surface area. Dissolution rates of pit edges measured in this study were normalized to the initial A of the {*hk*0} edges. However, dissolution rates of micas in the literature are normalized to initial BET-measured SA of particles, which includes both {00l} and {*hk*0} surfaces. To compare the rates calculated from an etch pit directly to rates reported in the literature, it is necessary to construct an imaginary particle with the same edge surface area as that of the etch pit. This was achieved by treating each etch pit as a "negative" particle with the same lateral dimensions as follows. An etch pit Z nanometers deep of area $A_{initial}$ expands to area A_{final} during time Δt. Assume this is equivalent to a particle Z nanometers thick of size A_{final} shrinking to size $A_{initial}$ during time Δt (Fig. 4). The equivalent particle is constructed so that

$$A_{total,initial} = 2A_{EP,final} + (Z \cdot P_{final}) \qquad [nm^2] \qquad (2)$$

$$A_{total,final} = 2A_{EP,initial} + (Z \cdot P_{initial}) \qquad [nm^2] \qquad (3)$$

where A_{EP} is the cross-sectional area of the etch pit and P is the etch pit perimeter. The total surface area determined in this way provides a geometric estimate of a BET equivalent surface area. Nonaka (1984) reports a roughness value (ratio of BET surface area to geometric surface area) for mica of 1.08, so this estimate of BET-equivalent surface area should be reasonable. Dissolution rates calculated from AFM images were then normalized to the total surface area of the equivalent particle for each etch pit. Dissolution rates normalized to {hk0} surface area and total surface area are reported in Table 1 for etch pits in contact with pH 2 HCl, and Table 2 for etch pits in contact with pH 5.7 distilled, deionized water equilibrated with atmospheric CO_2. The dissolution rates determined in this way are in the range of reported trioctahedral mica dissolution rates, while dissolution rates normalized to edge surface area are approximately 100 times faster (Fig. 5).

Table 1: Etch pit dimensions and dissolution rates for in situ AFM measurement of phlogopite dissolution in pH 2 HCl solution, including time (t), area (A), perimeter (P), volume (V), edge surface area ({*hk*0} SA), total surface area (Total SA), and dissolution rates based on edge surface area ({*hk*0} SA rate) and total surface area (Total SA Rate). Volume calculated assuming step height = 1.0 nm. Rates calculated with respect to initial pit volume. The error in measuring area and perimeter is approximately 5% and 10%, respectively. For pits with multiple layers, each layer was treated as individual etch pit. Asterisks (*) indicate that poor image quality prevented measurement.

Pit	(sec) t	(m^2) A	(m) P	(m^3) V	(m^2) {*hk*0} SA	(m^2) Total SA	(mol m^{-2} sec^{-1}) {*hk*0} SA Rate	(mol m^{-2} sec^{-1}) Total SA Rate
1	0	9.74E-14	1.26E-06	9.74E-23	1.26E-15	1.96E-13	------	------
1	54000	1.07E-13	1.35E-06	1.07E-22	1.35E-15	2.16E-13	4.94E-10	2.87E-12
1	140400	1.14E-13	1.42E-06	1.14E-22	1.42E-15	2.30E-13	3.25E-10	1.77E-12
1	226800	1.21E-13	1.49E-06	1.21E-22	1.49E-15	2.44E-13	2.85E-10	1.46E-12
1	313200	1.30E-13	1.64E-06	1.30E-22	1.64E-15	2.62E-13	2.83E-10	1.35E-12
2	0	1.57E-13	1.66E-06	1.57E-22	1.66E-15	3.16E-13	------	------
2	54000	*	*	*	*	*	*	*
2	140400	1.81E-13	1.84E-06	1.81E-22	1.84E-15	3.63E-13	3.42E-10	1.56E-12
2	226800	1.94E-13	1.88E-06	1.94E-22	1.88E-15	3.89E-13	3.26E-10	1.39E-12
2	313200	*	*	*	*	*	*	*
3	0	6.94E-14	1.15E-06	6.94E-23	1.15E-15	1.40E-13	------	------
3	54000	8.22E-14	1.26E-06	8.22E-23	1.26E-15	1.66E-13	6.96E-10	4.83E-12
3	140400	9.68E-14	1.35E-06	9.68E-23	1.35E-15	1.95E-13	5.71E-10	3.37E-12
3	226800	1.03E-13	1.40E-06	1.03E-22	1.40E-15	2.08E-13	4.36E-10	2.42E-12
3	313200	*	*	*	*	*	*	*
4	0	1.31E-14	4.65E-07	1.31E-23	4.65E-16	2.67E-14	------	------
4	54000	1.45E-14	4.92E-07	1.45E-23	4.92E-16	2.95E-14	1.86E-10	2.93E-12
4	140400	1.89E-14	5.77E-07	1.89E-23	5.77E-16	3.83E-14	2.97E-10	3.60E-12
4	226800	2.21E-14	6.20E-07	2.21E-23	6.20E-16	4.47E-14	2.86E-10	2.97E-12
4	313200	2.43E-14	6.20E-07	2.43E-23	6.20E-16	4.92E-14	2.58E-10	2.44E-12
5	0	1.78E-15	1.80E-07	1.78E-24	1.80E-16	3.74E-15	------	------
5	54000	2.58E-15	2.10E-07	2.58E-24	2.10E-16	5.38E-15	2.79E-10	9.34E-12
5	140400	5.39E-15	3.05E-07	5.39E-24	3.05E-16	1.11E-14	4.82E-10	7.83E-12
5	226800	6.55E-15	3.31E-07	6.55E-24	3.31E-16	1.34E-14	3.94E-10	5.29E-12
5	313200	7.69E-15	3.39E-07	7.69E-24	3.39E-16	1.57E-14	3.54E-10	4.05E-12

Table 2: Etch pit dimensions and dissolution rates for in situ AFM measurement of phlogopite dissolution in pH 5.7 dd-H_2O equilibrated with atmospheric CO_2. The symbols are the same as in Supplementary Table 1.

Pit	(sec) t	(m^2) A	(m) P	(m^3) V	(m^2) {*hk*0} SA	(m^2) Total SA	(mol m^{-2} sec^{-1}) {*hk*0} SA Rate	(mol m^{-2} sec^{-1}) Total SA Rate
1	0	1.45E-13	2.55E-06	1.45E-22	2.55E-15	2.93E-13	------	------
1	86400	1.54E-13	2.72E-06	1.54E-22	2.72E-15	3.10E-13	1.32E-10	1.09E-12
2	0	4.27E-14	8.70E-07	4.27E-23	8.70E-16	8.64E-14	------	------
2	86400	4.61E-14	9.38E-07	4.61E-23	9.38E-16	9.31E-14	1.49E-10	1.40E-12
3	0	1.43E-14	4.89E-07	1.43E-23	4.89E-16	2.91E-14	------	------
3	86400	1.64E-14	5.26E-07	1.64E-23	5.26E-16	3.32E-14	1.64E-10	2.42E-12
4	0	2.28E-14	6.39E-07	2.28E-23	6.39E-16	4.62E-14	------	------
4	86400	2.38E-14	6.39E-07	2.38E-23	6.39E-16	4.82E-14	6.14E-11	8.14E-13
5	0	4.44E-15	2.78E-07	4.44E-24	2.78E-16	9.16E-15	------	------
5	86400	5.55E-15	2.91E-07	5.55E-24	2.91E-16	1.14E-14	1.55E-10	3.8E-12
6	0	5.02E-15	2.93E-07	5.02E-24	2.93E-16	1.03E-14	------	------
6	86400	5.55E-15	2.93E-07	5.55E-24	2.93E-16	1.14E-14	7.03E-11	1.81E-12
7	0	1.96E-14	7.61E-07	1.96E-23	7.61E-16	3.99E-14	------	------
7	86400	2.25E-14	7.64E-07	2.25E-23	7.64E-16	4.58E-14	1.50E-10	2.49E-12
8	0	6.81E-15	3.69E-07	6.81E-24	3.69E-16	1.40E-14	------	------
8	86400	8.28E-15	3.86E-07	8.28E-24	3.86E-16	1.70E-14	1.56E-10	3.41E-12
9	0	1.21E-14	5.64E-07	1.21E-23	5.64E-16	2.47E-14	------	------
9	86400	1.57E-14	5.22E-07	1.57E-23	5.22E-16	3.20E-14	2.53E-10	4.47E-12
10	0	1.42E-14	5.23E-07	1.42E-23	5.23E-16	2.89E-14	------	------
10	86400	1.62E-14	6.28E-07	1.62E-23	6.28E-16	3.31E-14	1.50E-10	2.38E-12

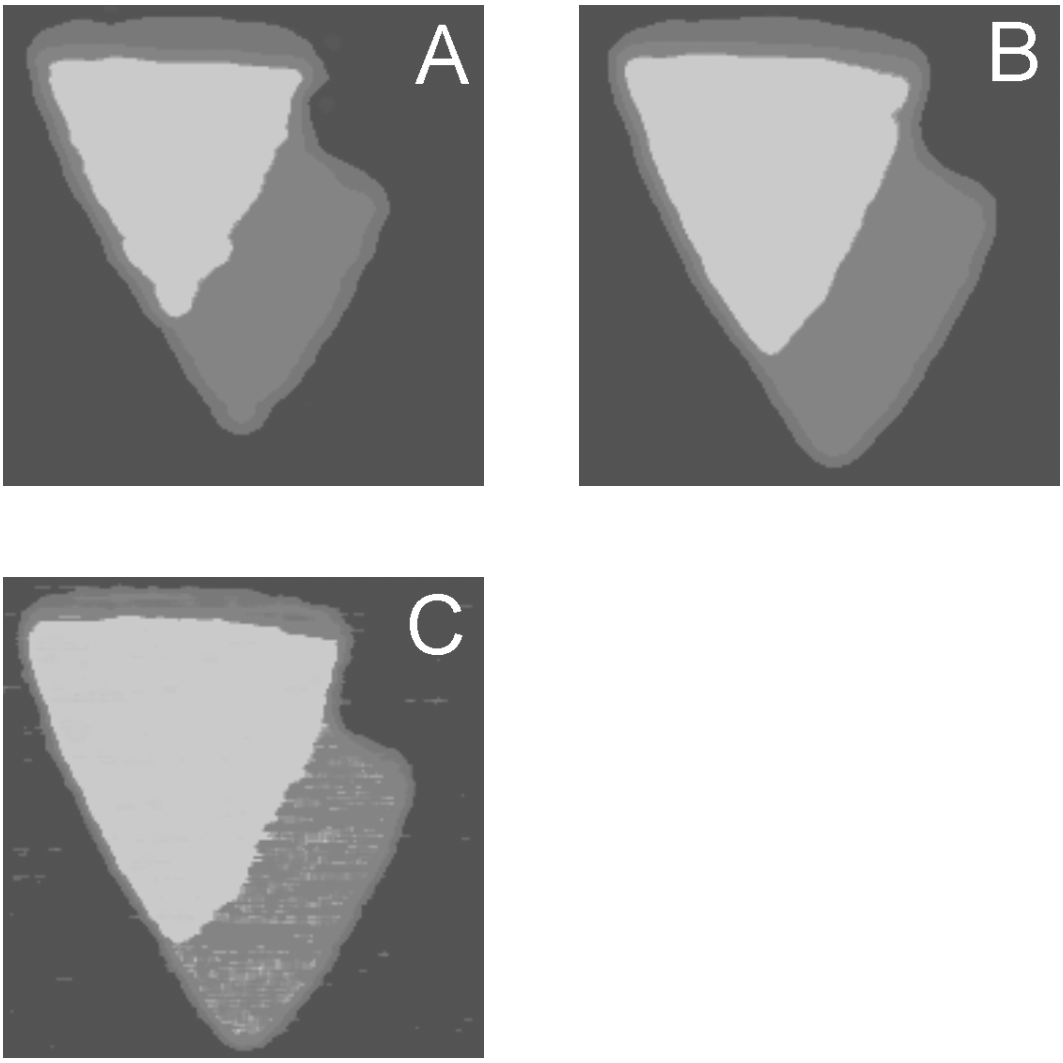

Figure 3: AFM image of phlogopite {001}. (A) After HF etch, showing typical initial morphology of etch pits. The darkest layer is the highest topographic layer (the original {001} surface before etching). Each successive lighter layer is 1.0 nm lower. The pits are triangular and flat bottomed. The same etch pit after (B) 39 hours and (C) 63 hours in contact with pH 2 HCl. All three images are the same scale, each image is 625 nm wide.

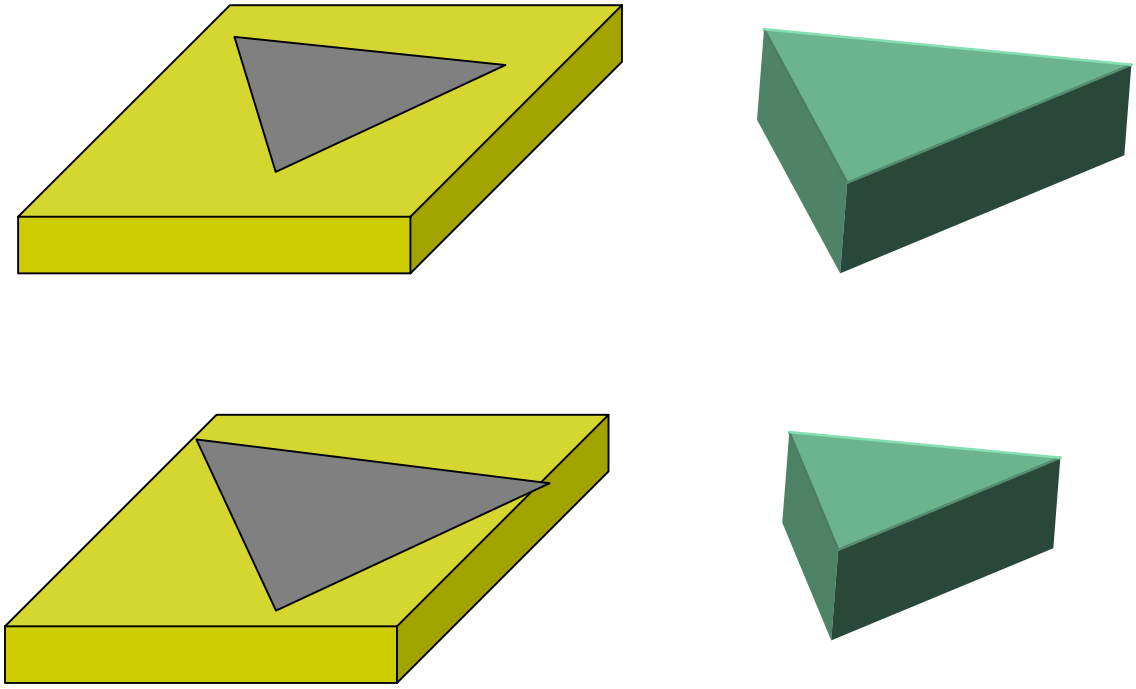

Figure 4: Construction of imaginary particle for dissolution rate calculations using Equations 2 and 3. Particle is constructed so that the final area, perimeter and volume are the same as the initial area, perimeter and volume of the etch pit. The etch pit and the particle experience the same volume loss during dissolution.

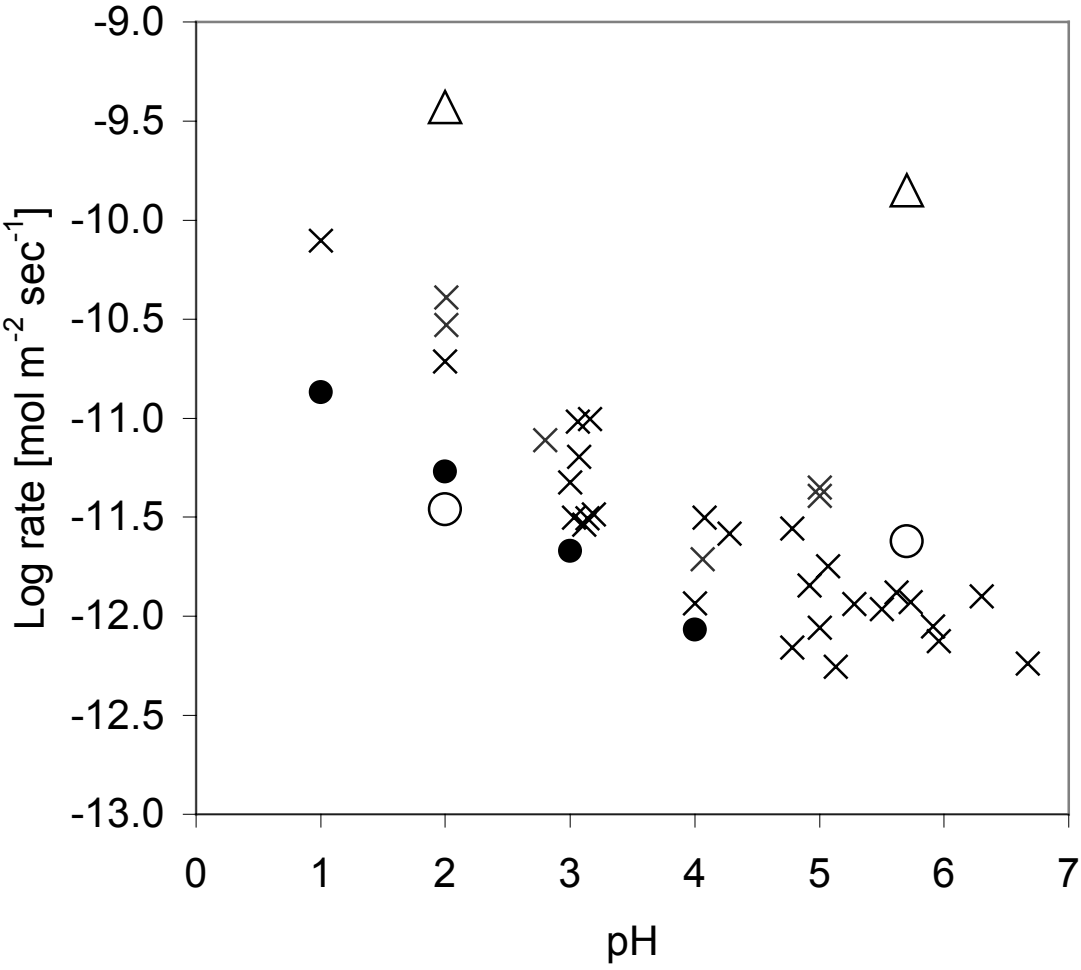

Figure 5: Comparison of phlogopite dissolution rates determined in this study (open circles and triangles) to reported phlogopite (filled circles; Kalinowski and Schweda, 1996) and biotite (×'s; Malmstrom and Banwart, 1997; Kalinowski and Schweda, 1996; Nagy, 1995 and references therein) dissolution rates. Dissolution rates of biotite (a closely related trioctahedral mica) are included because there are few published phlogopite rates. Open triangles indicate rates normalized to {*hk*0} edge surface area. Open circles indicate rates normalized to total surface area. Average {*hk*0} SA normalized rates are $3.7 \pm 1.3 \cdot 10^{-10}$ mol m^{-2} sec^{-1} at pH 2, and $1.4 \pm 0.5 \cdot 10^{-10}$ mol m^{-2} sec^{-1} at pH 5.7. Average total SA normalized rates are $3.5 \pm 2.3 \cdot 10^{-12}$ mol m^{-2} sec^{-1} at pH 2, and $2.4 \pm 1.2 \cdot 10^{-12}$ mol m^{-2} sec^{-1} at pH 5.7.

3.4 Long term dissolution of phlogopite (001)

Long-term, in situ AFM imaging was possible for phlogopite in contact with pH 2 HCl solution, and provides evidence of the reactivity of phlogopite {001} surfaces. At pH ~5.7, image quality degraded within 24 to 48 hours, precluding long term in situ experiments at this pH. Measured layer thickness of all layers exposed in a stepped etch pit (such as shown in Fig. 3) are reported in Table 3. Each layer is initially about 1.0 nm, corresponding to the thickness of one fundamental layer in the phlogopite structure. The layer thickness of the deeper layers remained constant during 127 hours in contact with pH 2 HCl. However, between 39 and 63 hours, the thickness of the top layer increased from ~1.0 nm to ~1.8 nm (Fig. 6). After 127 hours, tip-induced erosion was observed on the top layer only. Material was removed with continued scanning, leaving a persistent, uneven film with average thickness of about 1.2 nm. This increase in layer thickness was observed at 2 other locations on the sample surface and is a pervasive feature. It is unlikely that the solution in the fluid cell reached saturation with respect to a secondary phase, ruling out the possibility of precipitation accounting for the increase in layer thickness. High flow rate coupled with a slow dissolution rate prevented solution in the fluid cell reaching saturation with respect to secondary phases at pH 2. Reaching saturation with respect to amorphous silica, for example, would require > 100 layers of phlogopite to dissolve in static fluid filling the fluid cell. XPS performed after the sample was in contact with pH 2 HCl for 127 hours reveals that atomic concentrations of K, Al, Mg and F are severely depleted and the top layer is composed of essentially only Si and O. At 55°, Mg/Si decreases from 1.0 to 0.25 and Al/Si decreases form 0.33 to 0.21. K 2p and F 1s peaks are not discernable above background. Si/O increases from 0.22 to 0.49. Not surprisingly, LEED analysis performed on this sample yielded no diffraction spots, indicating that the surface region of the sample is now amorphous.

Table 3: Variation in layer thickness (Z) during in situ AFM observation of phlogopite dissolution in pH 2 HCl. Standard deviation (□) calculated from N AFM images analyzed. Layer thickness (step height) measured as peak separation in bearing curves, such as shown in Fig. 3. The thickness of the top layer (layer 1) shows considerable variability during 127 hours in contact with solution. Deeper layers (layers 2 and 3), exposed only within etch pits that penetrate layer 1, remain at ~1.0 nm.

		Layer 1 (Top Layer)		Layer 2		Layer 3	
(hours)		(nm)	(nm)	(nm)	(nm)	(nm)	(nm)
Time	N	Z	σ	Z	σ	Z	σ
0	8	1.01	0.04	1.05	0.06	1.07	0.04
15	5	1.17	0.03	1.09	0.05	1.08	0.03
39	8	1.06	0.05	1.02	0.05	1.10	0.05
63	8	1.74	0.03	1.03	0.05	1.07	0.02
87	10	1.86	0.09	1.02	0.09	1.09	0.11
127	6	1.20	0.06	0.98	0.06	1.05	0.06

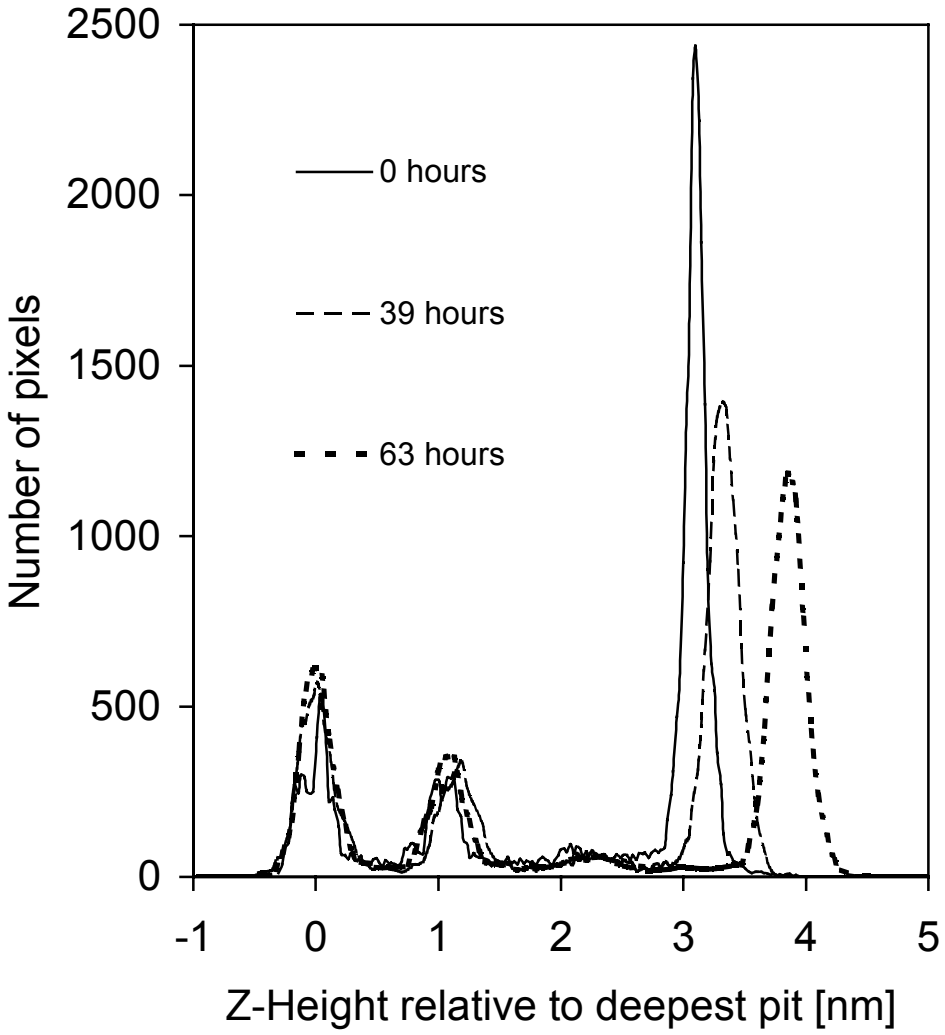

Figure 6: Distribution of topography in images shown in Figure 1. Z-height 0.0 is the topographic level corresponding to the floor of the etch pit seen in Figure 1. Peak separation measures step height (or layer thickness). The peaks at 0.0 and 1.0 nm remain constant, indicating that these deeper layers retain the same thickness. The peak representing the top layer shifts from 3.0 to 3.8 nm, indicating this layer has expanded from 1.0 to 1.8 nm in thickness.

The observed layer volume change may be explained by depolymerization and repolymerization reactions occurring during leached layer formation. The general leached layer model consists of three steps (Casey et al, 1993; Casey and Bunker, 1990). The first, sometimes referred to cation exchange, involves the rapid exchange of alkali and alkaline-earth cations for hydrogen or hydronium. The second involves depolymerization reactions, in which bridging Si-O-Si and Si-O-Al linkages are hydrolyzed, allowing the layer to expand. The third step is spontaneous repolymerization reactions in which neighboring Si-OH groups cross-link to reform Si-O-Si linkages, ejecting hydrogen and water. This may cause the layer to contract, leading to the observed tip induced sample erosion.

Mica dissolution is thought to be dominated by an edge attack mechanism (Malmstrom and Banwart, 1997; Kalinowski and Schweda, 1996; Nagy, 1995 and references therein). In acidic solution, interlayer and octahedral cations are selectively leached through {*hk*0} surfaces forming an altered silica-enriched rim. Dissolution reaches steady state when the removal of silica from the altered edges is matched by diffusion of interlayer and octahedral cations parallel to the sheets, through the altered rim. However, acid hydrolysis studies of expandable clays provide evidence for leaching of octahedral cations perpendicular to the sheets, through the ditrigonal cavities of the {001} surface by a mechanism referred to as gallery access (Kaviratna and Pinnavaia, 1994). Our observations that the {001} surface undergoes a compositional change and expansion indicate that exposed {00l} surfaces also participate in the dissolution process, at least initially.

Chapter 4: Conclusions

This study has provided directly measured dissolution rates for surfaces on phlogopite, a silicate mineral, at room temperature. It has also shown that all phlogopite surfaces are reactive, including its basal surfaces. Each surface of phlogopite, or any other mineral, must behave according to the particular atomic structure, composition and microtopography of that surface. Furthermore, the dissolution of each surface has a temporal dependence, although this effect may only be significantly variable in the early stages of dissolution. Finally, external factors must also come into play (for example, local conditions and proximal flow regimes), especially in natural settings (Hochella and Banfield, 1995). The concept and use of reactive surface area in silicate dissolution studies is now changing. It seems that, at least in the most favorable cases, the reactivity of various surface components can be cataloged and quantified. This opens the door to a new generation of rate equations and, ultimately, to a much better understanding of how minerals dissolve and influence our environment.

REFERENCES

Bloss, F.D., Gibbs, G.V., and Cummings, D. (1963) Polymorphism and twinning in synthetic fluorophlogopite. J. Geology 71: 537-547.

Barrett S.D., Bickmore B.R., Rufe E, Hochella M.F. Jr., Torzo, G., and Cerolini, D. (2000) The use of macros in AFM image analysis and image processing. (submitted to Journal of Computer Assisted Microscopy).

Bickmore B.R., Bosbach D., Hochella M.F. Jr., Charlet L. and Rufe E. (2000) In situ atomic force microscopy study of hectorite and nontronite dissolution: Implications for phyllosilicate edge structures and dissolution mechanisms (submitted to American Mineralogist).

Bickmore B.R., Rufe E., Barrett S.D., and Hochella M.F. Jr. (1999) Measuring discrete feature dimensions in AFM Images with Image SXM. Geological Materials Research. 1(5). [http://gmr.minsocam.org].

Bosbach D., Charlet L., Bickmore B.R., Hochella M.F. Jr. (2000) The dissolution of hectorite: In-situ, real-time observations using Atomic Force Microscopy. Am Min 85, 1209-1216.

Brantley S.L. and Chen Y. (1995) Chemical weathering rates of pyroxenes and amphiboles. In: Chemical Weathering Rates of Silicate Minerals (A.F. White and S.L. Brantley, eds) Reviews in Mineralogy Vol. 31: 119-172.

Casey W.H. and Bunker B. (1990) Leaching of mineral and glass surfaces during dissolution. In: Mineral-Water Interface Geochemistry (M.F. Hochella Jr. and A.F. White, eds) Reviews in Mineralogy Vol 23: 397-426.

Casey W.H., Westrich H.R. and Arnold G.W. (1988) Surface chemistry of labradorite feldspar reacted with aqueous solutions at pH = 2, 3 and 12. Geochim Cosmochim Acta 52, 2795-2807.

Casey W.H., Westrich H.R., Banfield J.F., Ferruzzi G. and Arnold G.W. (1993) Leaching and reconstruction at the surfaces of dissolving chain-silicate minerals. Nature 366: 253-256.

Cetisli, H., and Gedikbey, T. (1990) Dissolution kinetics of sepiolite from Eskisehir (Turkey) in hydrochloric and nitric acids. Clay Mineral 25: 207-215.

Drever J.I. and Clow D.W. (1995) Weathering Rates in Catchments. In: Chemical Weathering Rates of Silicate Minerals (A.F. White and S.L. Brantley, eds) Reviews in Mineralogy Vol. 31: 463-484.

Hochella, M.F. Jr. (1988) Auger electron and X-ray photoelectron spectroscopies. In Spectroscopic Methods in Mineralogy and Geology (F.C. Hawthorne, Ed.) Reviews in Mineralogy Vol. 18: 573-637.

Hochella, M.F. Jr. (1995) Mineral surfaces: their characterization and their chemical, physical and reactive nature. In: Mineral Surfaces (D.J. Vaughan and R.A.D. Pattrick, eds) The Mineralogical Society Series 5: 17-60.

Hochella, M.F. Jr. and Banfield J.F. (1995) Chemical weathering of silicates in nature: A microscopic perspective with theoretical considerations. In: Chemical Weathering Rates of Silicate Minerals (A.F.White and S.L. Barnatley, eds) Reviews in Mineralogy Vol. 31: 353-406.

Hochella M.F. Jr. and Carim A.F. (1988) A reassessment of electron escape depths in silicon and thermally grown silicon dioxide thin films. Surface Sci 197: L260-L268.

Hochella M.F. Jr., Rakovan J.F., Rosso K.M., Bickmore B.R. and Rufe E. (1998) New directions in mineral surface geochemical research using scanning probe microscopy In Mineral-Water Interfacial Reactions: Kinetics and Mechanisms, vol. 715 of ACS Symposium Series (D.C. Sparks and T.J. Grundl, Eds) 37-56.

Jordan G. and Ramansee W. (1996) Dissolution rates and activation energy for dissolution of brucite (001): A new method based on the microtopography of crystal surfaces. Geochim Cosmochim Acta 60: 5055-5062.

Jordan G., Higgins S.R., Eggleston C.M., Swapp S.M., Janney D.E. and Knauss, K.G. (1999) Acidic dissolution of plagioclase: In-situ observations by hydrothermal atomic force microscopy. Geochim Cosmochim Acta. 63: 3183-3192.

Kalinowski B.E. and Schweda P. (1996) Kinetics of muscovite, phlogopite, and biotite dissolution and alteration at pH 1-4, room temperature. Geochim Cosmochim Acta 60: 367-385.

Kaviratna, H. and Pinnavaia, T.J. (1994) Acid hydrolysis of octahedral Mg^{2+} sites in 2:1 layered silicates: An assessment of edge attack and gallery access mechanisms. Clays Clay Min 42: 717-723.

Koretsky C.M., Sverjensky D.A. and Sahai N. (1998) Surface site types on oxide and silicate minerals based on crystal chemistry: Implications for site densities, multisite adsorption, surface infrared spectroscopy and dissolution kinetics. Am J Sci 298: 394-438.

Liang Y., Baer D.R. and Lea A.S. (1995) Dissolution of CaCO3 (1014) surface. Mat Res Soc Symp Proc Vol 355: 409-414.

Malmstrom M. and Banwort S. (1997) Biotite dissolution at 25 C: The pH dependence of dissolution rate and stoichiometry. Geochim Cosmochim Acta 61: 2779-2799.

McCauley, J.W., Newnham, R.E. and Gibbs, G.V. (1973) Crystal structure analysis of synthetic fluorophlogopite. Am Min 56: 249-254.

Medina, J.A., Morante, M., Leguey, S. Tornero, J. (1985) Some observations on the relationship between etch-pit form and structure in biotite. Clay Minerals 20: 263-271.

Nagy K.L. (1995) Dissolution and precipitation kinetics of sheet silicates. In Chemical Wethering Rates of Silicate Minerals (A.F.White and S.L. Barnatley, eds) Reviews in Mineralogy Vol. 31: 173-233.

Nonaka A. (1984) J Colloid Interf Sci 99: 335.

Patel, A.R. and Ramanathan, S. (1962a) Etching of mica cleavages. Acta Crystallographica 15; 860-862.

Patel, A.R. and Ramanathan, S. (1962b) Etching of synthetic fluorophlogopite. American Mineralogist 47: 1195-2001.

Pouchou J.L. and Pichoir, F. (1985) "PAP" procedure for improved quantitative microanalysis. Microbeam Analysis. 20: 104-105.

Putnis A., Junta-Rosso J.L. and Hochella M.F. Jr. (1995) Dissolution of barite by a chelating ligand: An atomic force microscopy study. Geochim Cosmochim Acta 59: 4623-4632.

Rufe E. and Hochella M.F. Jr. (1999) Quantitative assessment of reactive surface area of phlogopite during acid dissolution. Science 285: 874-876.

Russ J.C. (1999) The Image Processing Handbook. 3d Edition, CRC Press, Boca Raton, FL. 771 pp.

Stipp, S.L. and Hochella, M.F. Jr. (1991) Structure and bonding environments at the calcite surface as observed with X-ray photoelectron spectroscopy (XPS) and low energy electron diffraction (LEED). Geochim Cosmochim Acta. 55: 1726-1736.

Turpault, M.-P. and Trotignon, L. (1994) The dissolution of biotite single crystals in dilute HNO_3 at 24 °C: Evidence of an anisotropic corrosion process of micas in acidic solutions. Geochim Cosmochim Acta 58: 2761-2775.

Wagner C.D., Passoja D.E., Hillery H.F., Kinisky T.G., Six H.A., Jansen W.T., and Taylor J.A. (1982) Auger and photoelectron line energy relationships in aluminum-oxygen and silicon-oxygen compounds. J. Vac. Sci. Tech. 21: 933-944.

White A.F. and Brantley S.L. (1995) Chemical Weathering Rates of Silicate Minerals (A.F.White and S.L. Barnatley, eds) Reviews in Mineralogy Vol. 31: 565-583.

White A.F. and Peterson ML (1990) Role of reactive-surface-area characterization in geochemical kinetic models. In: Chemical Modeling of Aqueous Systems II. Am Chem Soc Symp Series 416: 461-475.

Vita

A native of Eastern Pennsylvania, the author received a B.S. in 1994 from the Department of Geosciences at the Pennsylvania State University before coming to Virginia Polytechnic Institute and State University. Like many native Eastern Pennsylvanians, the author is wary of the internet, and prefers not to divulge too much biographical information in cyberspace.